RSC Advances

Chitosan (PEO)/bioactive glass hybrid nanofibers for bone tissue engineering

Journal:	*RSC Advances*
Manuscript ID:	RA-ART-07-2014-006761.R1
Article Type:	Paper
Date Submitted by the Author:	07-Sep-2014

Complete List of Authors:	Talebian, Sepehr; University of Malaya, Mechanical Engineering Mehrali, Mehdi; University Of Malaya, Mohan, Saktiswaren; University of Malaya, mechanical Engineering raghavendran, Hanumanth rao; Liver and immunology research centre , Mehrali, Mohammad; University of Malaya, Mechanical Engineering Mohammad Khanlou, Hossein; University of Malaya, mechanical Engineering Kamarul, Tunku; University of Malaya, Orthopedic Surgery Muhammad Afifi, Amalina; University of Malaya, mechanical Engineering

Table of contents entry

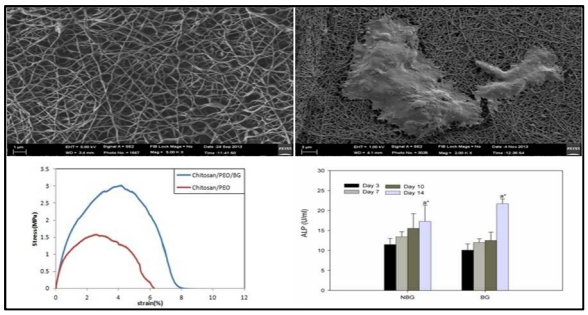

Incorporation of bioactive glass into chitosan(PEO) nanofibers leads to improvement of strength and bone-cell differentiation capability.

Cite this: DOI: 10.1039/c0xx00000x

www.rsc.org/xxxxxx

ARTICLE TYPE

Chitosan (PEO)/bioactive glass hybrid nanofibers for bone tissue engineering

Sepehr Talebian[a,*], Mehdi Mehrali[a], Saktiswaren Mohan[b], Hanumantha rao Balaji raghavendran[b], Mohammad Mehrali [a], Hossein Mohammad Khanlou[a], Tunku Kamarul[b], Amalina Muhammad Afifi[a,*]

A novel hybrid nanofibrous scaffold prepared with chitosan [containing 1.2 wt% polyethylene oxide (PEO)] and bioactive glass (BG) was fabricated by an electrospinning technique. The morphological and physicochemical properties of scaffolds were studied by scanning electron microscopy (SEM) and spectroscopy. The measurements of tensile strength and water-contact angles suggested that the incorporation of BG into the nanofibers improves the mechanical properties and hydrophilicity of the scaffolds. Biomineralization of the nanofibers was evaluated by soaking them in simulated body fluid (SBF), and the formation of hydroxycarbonate apatite (HCA) layer was determined by EDX and FE-SEM. The results showed that BG-containing nanofibers could induce the formation of HCA on the surface of composite after 14 days of immersion in SBF. *In vitro*-cell viability of human mesenchymal stromal cells (hMSCs) on nanofibers was assessed by using the MTT assay. The cell-adhesion results showed that hMSCs were viable at variable time points on the chitosan/PEO/ BG nanofiber scaffolds. In addition, the presence of BG enhanced the alkaline phosphatase (ALP) activity of hMSCs cultured on composite scaffolds at day 14 as compared to that on pure chitosan/PEO scaffolds. Our results suggest that chitosan/PEO/BG nanofibrous composite could be a potential candidate for application in tissue engineering.

Introduction

The major bone extracellular matrix (ECM) building blocks are composed of collagen I fibrils (50–500-nm diameter) mineralized with a thin, highly crystalline carbonated apatite layer. Therefore, a biodegradable, highly porous, strong nanofibrous scaffold that mimics the collagen fibrils is highly recommended for use in the field of bone tissue engineering for promoting osteoblasts infiltration and proliferation [1, 2]. Electrospun nanofibers are a promising materials for bone tissue engineering owing to their morphological similarity with that of bone ECM, large "surface area/volume" ratio that offers a larger space for cell adhesion and proliferation, and a tunable porous structure that provides a favorable site for drug release and ion exchange *in vitro* and *in vivo* [3, 4]. It has been reported that the biological features of electrospun nanofibrous scaffolds including biocompatibility, bioactivity, hydrophilicity, and mechanical properties are mainly dependent on the selected polymer material [5].

Meanwhile, chitosan, a polysaccharide obtained by partial deacetylation of chitin, has a linear structure and is composed of randomly distributed β-(1-4)-linked D-glucosamine (deacetylated section) and N-acetyl-D-glucosamine (acetylated section). It plays important roles in the attachment, differentiation, and morphogenesis of osteoblast cells owing to its structural similarity to that of glycosaminoglycans (GAG), which is a major bone and cartilage component [6-8]. Nevertheless, lack of bioactivity and low mechanical strength limits the application of biopolymers in bone regenerative scaffolds [9]. To overcome these drawbacks of biopolymers, a variety of bioactive inorganic materials have been incorporated into the polymer matrix (by a composite approach) to improve the biological properties (such as bioactivity, protein adsorption, cell proliferation, and osteogenic differentiation) and the mechanical strength of the resulting biocomposite [10-16].

Among the inorganic phases, bioactive glasses (BGs) are quite fascinating because immersing BG in a body fluid initiates formation of amorphous calcium phosphate on their surface, which later crystallizes into a hydroxyl carbonate apatite (HCA) layer. This HCA layer mimics the chemical composition and structure of bone mineral and plays a key role in forming a bond with the surrounding bone tissues [5, 6, 9, 17-21]. The combination of chitosan/BG as a composite scaffold is a new and promising approach for bone cell regeneration, with only few supporting literature [10, 22, 23]. However, to the best of our knowledge, bone cell regeneration using electrospun chitosan (polyethylene oxide; PEO)/BG nanofibrous composite is the first of its kind approach that can pave the way toward the development of a novel bone tissue regenerative scaffold for repairing bone defects. For this purpose, an electrospinning technique was employed to fabricate a novel nanofibrous nanocomposite membrane from chitosan/PEO solution incorporating BG particles. Various properties of the nanocomposite membrane including mechanical

properties, wettability, and biomineralization were investigated. In addition, detailed *in vitro* biological assessments were performed, such as cell adhesion, cell viability [3-(4,5-dimethylthiazol-2-yl)-2,5-diphenyltetrazolium bromide; MTT assay], and bone cell differentiation [alkaline phosphatase (ALP)] to evaluate the efficiency of nanofibrous scaffold for bone repair.

Results and Discussion

Morphology of electrospun nanofibers

Figure 1 shows the FE-SEM images of electrospun chitosan/PEO and chitosan/PEO/BG nanofibers. The original chitosan/PEO nanofibers were smooth fine fibers with random orientation on the collector. However, after addition of BG powders, in some areas the fibers started to fuse together (adjacent fiber adhered together from their interface) due to the formation of secondary bonding (hydrogen bonds and ionic bonds) [24]. Moreover, in some regions, small particles of BG were located on the surface of fibers, which imparted roughness to the fibers[2].

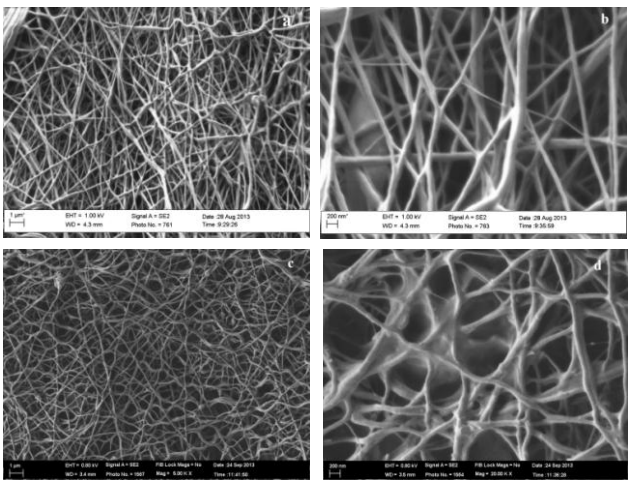

Figure 1. FESEM images of chitosan/PEO (a, b) and chitosan/PEO/BG (c, d) scaffolds.

Evaluation of BG particles in chitosan/PEO/BG nanofibers

Three independent characterization methods—XRD, FTIR, and EDX—were used to characterize the nanofibrous membranes, particularly the BG particle deposits on the surface of chitosan/PEO/BG nanofibers. Figure 2 shows the XRD and FTIR spectra of BG powders and the electrosopun nanofibers.

The X-ray diffractograms revealed that the BG powders formed sodium calcium silicate ($Na_2CaSi_3O_8$) and $Na_2Ca_2Si_3O_9$, which coincides with sodium calcium silicate in the JCPDS card 012-0671 and 022-1455, respectively[19, 25-29]

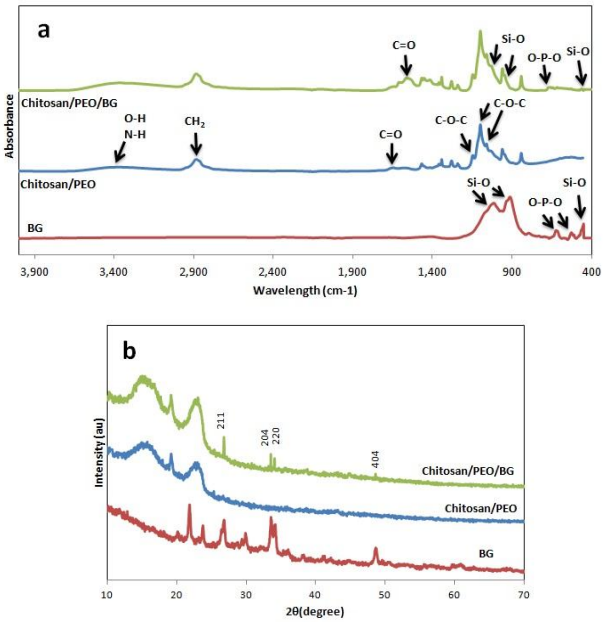

Figure 2. Characterizations of BG and electrospun nanofibers. (a) FTIR spectrums. (b) XRD spectrums.

The XRD pattern of chitosan/PEO shows the crystalline nature of these nanofibers, consisting of three peaks. The sharp peak at 2θ of 19° and the broad peak at 2θ of 23° are attributed to the crystalline phase of PEO, and the one broad peak at 2θ of 15° is assigned to the crystalline phase of chitosan [30]. The addition of BG to the nanofibers introduces four extra peaks to the pattern that are related to the crystalline phase of BG ($Na_2Ca_2Si_3O_9$); peak at 2θ of 26° is attributed to 211 crystal plane, peaks at 2θ of 33° and 34° are attributed to 204 and 220 crystal planes, respectively, and the peak at 2θ of 48° is attributed to 404 crystal plane [27-29]. The FTIR spectra of pure BG powder showed the absorption bands of 527 cm^{-1} and 624 cm^{-1} assigned to the bending vibrations of the O-P-O groups. The three peaks at 451, 913, and 1014 cm^{-1} were allocated to the stretching vibration of Si-O bonds in each SiO_4 tetrahedron [6, 10, 26, 31-34]. In chitosan/PEO FTIR spectra, the triple bands at 1061, 1099, and 1146 cm^{-1} were assigned to the stretching vibration (ν_s) of the C-O-C groups and, together with the band at 2883 cm^{-1} (CH_2 stretching), they were considered as the characteristics peaks of PEO. In the same spectra, the broad band at 3362 cm^{-1} was allocated to N-H and O-H stretching of polysaccharide molecules. Furthermore, the absorption band at 1645 cm^{-1} was attributed to the stretching vibration of amide I groups (canbonyl, C=O-NHR) in the chitosan. Finally, the FTIR spectra of chitosan/PEO/BG nanofibers revealed the bands at 463 and 659 cm^{-1} that did not appear in the chitosan/PEO spectra, which have been assigned to the Si-O stretching band and the O-P-O bending band, respectively. In addition, broadening of the band at approximately 961 and 1060 cm^{-1}, in conjunction with a slight shift of amid I band to 1563 cm^{-1}, were attributed to the interaction of chitosan with BG [6, 10, 35-37].

Finally, the elemental analysis (EDX) (Figure 3a) of the chitosan/PEO/BG nanofibers showed large peaks of carbon and oxygen indication of the two main components of chitosan and PEO, in addition small amounts of silicon, calcium and sodium were indication of BG particles in the scaffolds. Moreover, EDX mapping results revealed the distribution of carbon (Figure 3b) and oxygen (Figure 3c) as the major organic components of scaffolds whereas the inorganic sodium (Figure 3d), silicon (Figure 3e) and calcium (Figure 3f) were observed in the form of BG particles on fibres. It is worth noting that silicon as the major component of BG particles showed several large bright spots on the EDX map (Figure 3e) (that is also observable in Figure 3a as white particles), which implies to heterogeneous distribution of BG particles in some areas of the nanofiber membrane.

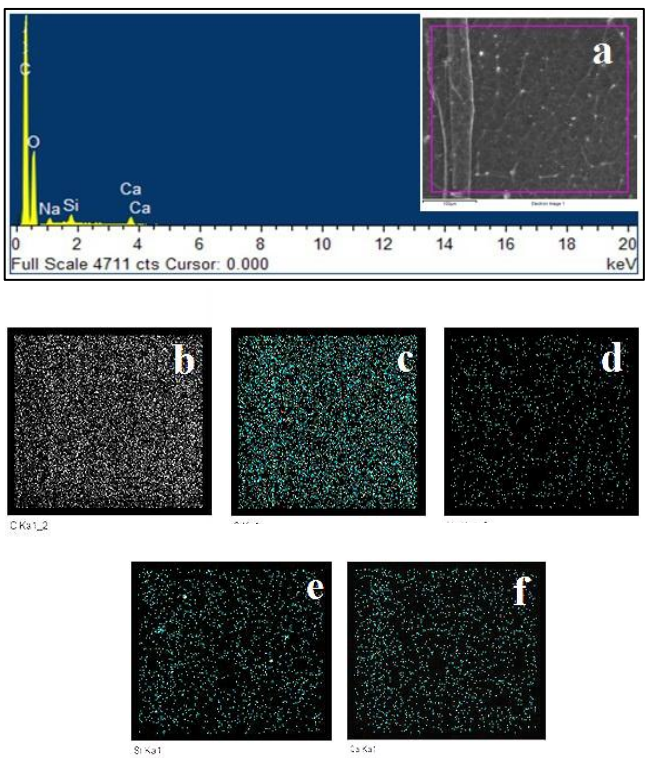

Figure 3. EDX spectra of chitosan/PEO/BG composite nanofibers (a). Elemental mapping representing the elemental distribution of carbon (b), oxygen (c), sodium (d), silicon (e) and calcium (f) of the composite nanofibers.

Mechanical properties of electrospun nanofibers

The stress–strain curves of chitosan/PEO and 1% (w/v) chitosan/PEO/BG nanofibers are given in Figure 4. The average tensile strength of chitosan/PEO nanofibers was 1.58 ± 0.2 MPa with strain at break of 2.5%, whereas chitosan/PEO/BG nanofibers had a tensile strength of 3.01 ± 0.15 MPa with strain at break of 4%. Accordingly, the 1%-loaded nanofibers showed a higher tensile strength than pristine chitosan/PEO nanofibers, due to the formation of secondary bonds between BG particles and the matrix [6]. Moreover, the composite nanofibers exhibited better ductility as a result of yielding phenomenon, which is the consequence of debonding between BG particles and chitosan/PEO matrix [38].

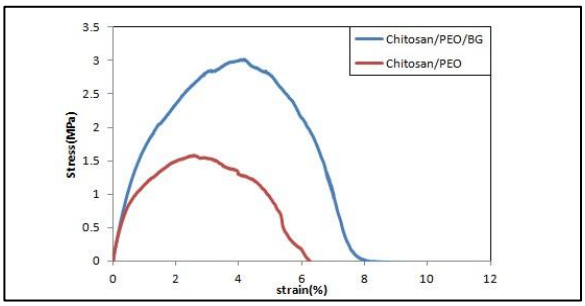

Figure 4. Stress-strain curves of chitosan/PEO and chitosan/PEO/BG nanofibers.

Wettability of electrospun nanofibers

Cell–scaffold interactions are strongly influenced by the wettability of the scaffold's surface, because this property determines some of the most significant biological events such as protein adsorption, cell attachment, and cell proliferation [10]. The water-contact angle of chitosan/PEO and chitosan/PEO/BG nanofibers was measured to evaluate the wettability of the scaffolds (Figure 5). The chitosan/PEO membranes had a contact angle of 57.5 ± 4°, while the BG-containing membranes possessed a contact angle of 38.1 ± 2°. This difference implies that the BG-containing nanofibers possessed a higher hydrophilicity. The exposure of BG particles on the surface of fibers creates a relatively rough and more hydrophil surface, which imparts better wettability of these composite fibers [38].

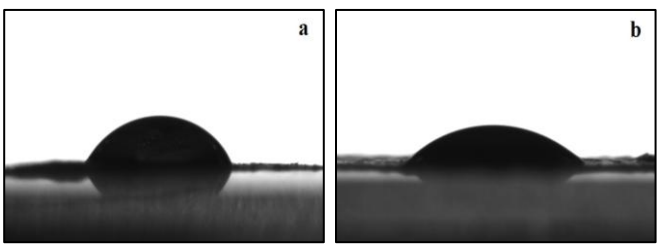

Figure 5. Water contact angle of chitosan/PEO (a) and chitosan/PEO/BG (b) nanofibers.

Biomineralization of electrospun nanofibers with respect to apatite formation

The bone-bonding capability of a scaffold is sometimes assessed by its ability to induce apatite formation on its surface upon immersion in SBF [39] (apart from few exceptions where the materials directly bonded to living bone without the formation of detectable apatite on their surface[39]). The response of electrospun nanofibers in contact with SBF was evaluated by FE-SEM and EDX. FE-SEM micrographs of electrospun chitosan/PEO and chitosan/PEO/BG membranes soaked in SBF for 14 days are shown in Figure 6a–d. After soaking in SBF, on both BG-containing and non-BG-containing nanofibers, a calcium

phosphate layer was observed. In BG-containing nanofibers a layer of plate-like apatite with approximate thickness of 100-150 nm formed on their surface that was developed perpendicular to the fibers surface. Furthermore, based on the EDX spectra of chitosan/PEO/BG nanofibers after incubation with SBF (Figure 6f), the presence of calcium and phosphorous on their surface was confirmed, and the Ca/P molar ratio of the coating was estimated to be 1.53, which is lower than that of stoichiometric hydroxyapatite (Ca/P = 1.67), but similar to that of hydroxycarbonate apatite (HCA) (Ca/P = 1.5) [34, 35]. Previously it has been reported that formation of apatite on artificial scaffolds is induced by incorporation of functional groups that could create negative charge on the scaffold. Thus, BG particles in chitosan/PEO/BG nanofibers act as nucleation initiation sites for formation of apatite, leading to faster formation of more apatite [40]. On the other hand, non-BG-containing nanofibers showed a significantly different morphology of calcium phosphate deposition on their surface. In these nanofibers the calcium phosphate layer didn't appear as plate-like apatite, instead it was emerged as a smooth layer (with approximate thickness of 50nm) covering the fibre surface causing the average fiber diameter to increase to 100-150nm. In addition, The EDX spectra of chitosan/PEO nanofibers after incubation with SBF (Figure 6e) showed negligible amount of Ca and P (comparing to chitosan/PEO/BG nanofibers) with Ca/P molar ratio of 0.65, which is far lower than that of stoichiometric hydroxyapatite (Ca/P = 1.67) but closer to that of calcium pyrophosphate (Ca/P = 1)[41]. It is worth noting that presence of positively charged amino groups on the back bone of chitosan together with absence of apatite nucleation initiators could cause a reduction in apatite forming ability of chitosan/PEO nanofibers and lowers the Ca/P ratio[35, 40].

These results suggest that chitosan/PEO/BG nanofibers show improved apatite forming ability compared to chitosan/PEO nanofibers when immersed in SBF and therefore they might be ideal for forming a bond with bone[39].

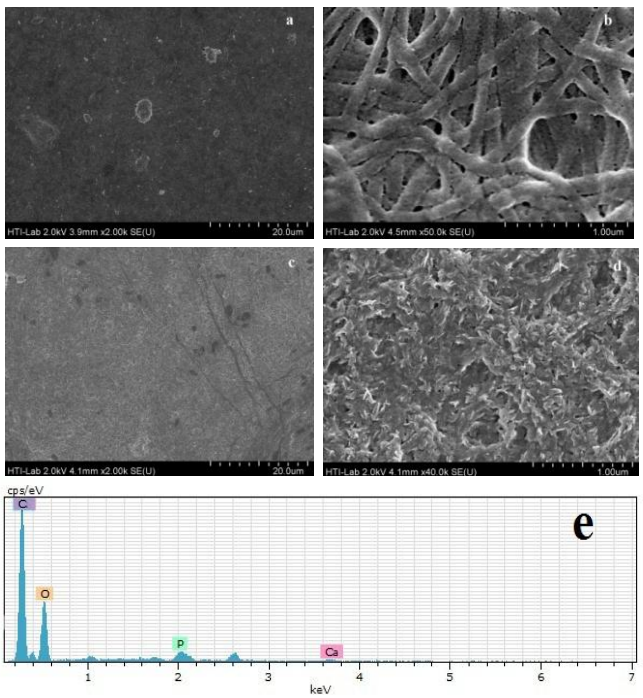

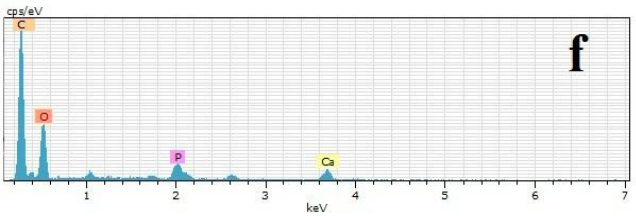

Figure 6. Characterizations of nanofibers surface after 14 days incubation in SBF at 37°C. FESEM images of chitosan/PEO (a, b) and chitosan/PEO/BG (c, d) nanofibers surface after immersion in SBF. EDX spectra of calcium phosphate layer formed on the surface of chitosan/PEO (e) and chitosan/PEO/BG (f) nanofibers after immersion in SBF.

Cell adhesion and viability

Initial attachment and adhesion of hMSCs are extremely crucial for their long-standing stability and differentiation [42]. In our study, we investigated the cellular behavior by fluorescence microscopy and MTT assay to evaluate cell adhesion and viability in order to correlate the properties of scaffolds and the cultivated cell response. Furthermore, FE-SEM was used to visualize the morphological changes in hMSCs during culturing. The cell viability at different time points was confirmed by the MTT assay; however, no statistically significant difference was noted between chitosan/PEO and chitosan/PEO/BG scaffolds. These results indicate that these scaffold materials did not interfere with cell viability and hence were not cytotoxic.

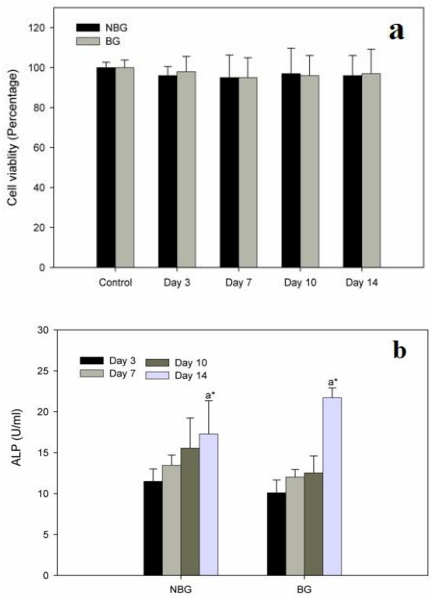

Figure 7. MTT viability assay (a) and ALP activity (b) of hMSCs measured on chitosan/PEO/bioactive glass scaffolds (BG) and chitosan/PEO scaffolds (NBG) after 3, 7, 10 and 14 days of cultivation.

Consistent with the cell-viability assay, Hoechst staining also confirmed that cells were viable at every tested time points in the scaffolds. The blue-stained cells were observed on all scaffolds, which indicated that the composition of the scaffolds provided a physiological environment for cell attachment and, thus, the

scaffolds were biocompatible. The MTT results and fluorescence microscopy images are shown in **Figure 7a** and **Figure 8-9**, respectively.

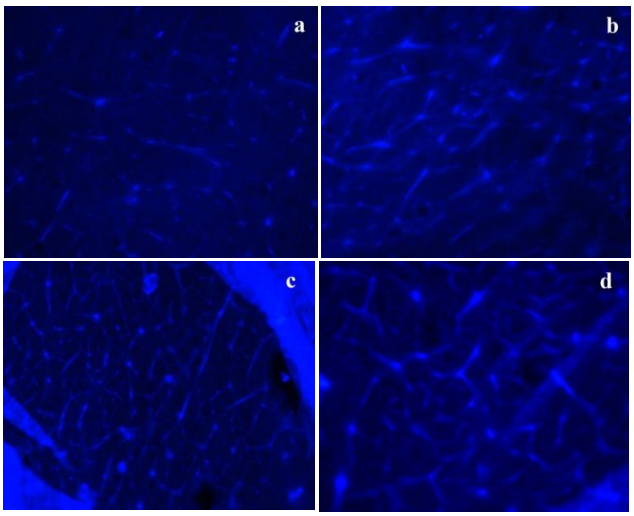

Figure 8. Fluorescence microscope images of adherent hMSCs on chitosan/PEO scaffolds after 1(a), 3(b), 5(c) and 7(d) days.

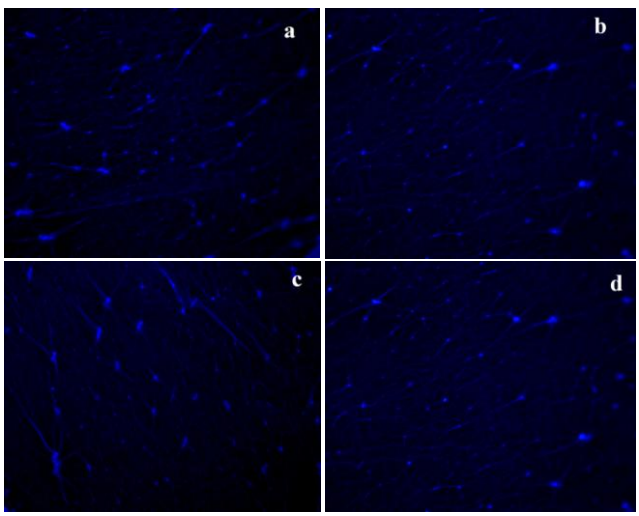

Figure 9. Fluorescence microscope images of adherent hMSCs on chitosan/PEO/BG scaffolds after 1(a), 3(b), 5(c) and 7(d) days.

The SEM images of MSCs after 1, 3, 5, and 7 days of culturing on the scaffolds are demonstrated in Figure 10-11. The SEM results complimented the fluorescence microscopy results, indicating that MSCs adhere and spread on the nanofiber scaffolds. From day 1, the cells started to spread on the nanofiber scaffolds and tended to show filopodia extending toward the adjacent cells. This filopodia extension continues until the 7^{th} day, by when the adjacent cells adhere to each other to form tight clusters. Moreover, with time, the number of cells adhered to the scaffold surface increases, indicating that these scaffolds are good supporters of the cells.

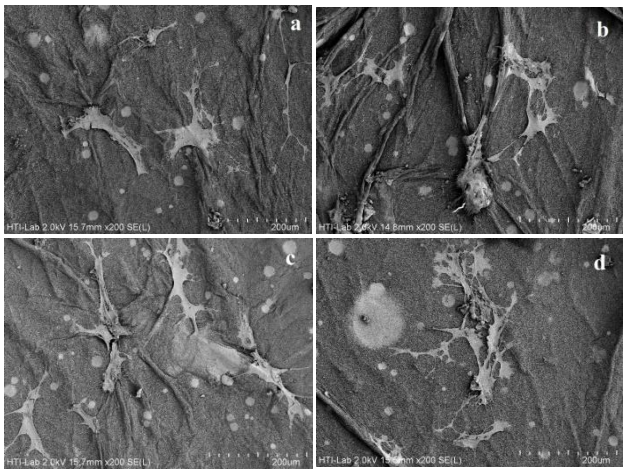

Figure 10. FESEM images of hMSCs cultured on the chitosan/PEO scaffolds after 1(a), 3(b), 5(c) and 7(d) days.

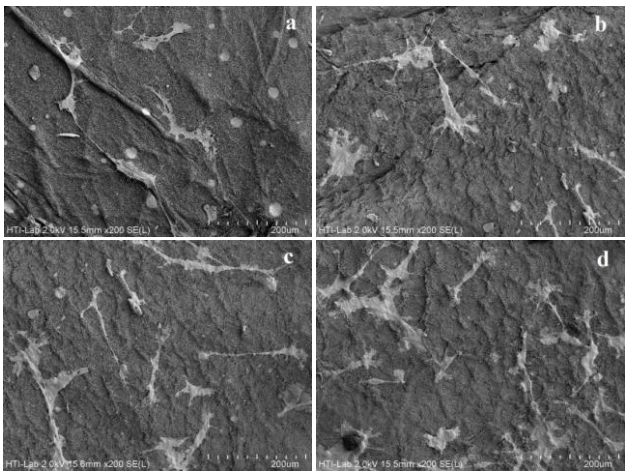

Figure 11. FESEM images of hMSCs cultured on the chitosan/PEO/BG scaffolds after 1(a), 3(b), 5(c) and 7(d) days.

Cell differentiation and mineralization

An efficient bone scaffold should be able to support bone formation, including the organic and inorganic constituents on the natural tissue. ALP is considered to be one of the major components of the bone tissue vesicles owing to its role in the formation of calcium phosphate-containing apatite. In addition, ALP is a well-know early stage marker of osteogenic differentiation. The ALP activity results are shown in Figure 7b. Consequently, the ALP activity gradually increased 2-fold in cells cultured in the chitosan/PEO/BG scaffold by day 14 as compared to that at the early time points ($P < 0.05$). Although a gradual increase in ALP was noted in the cells cultured in chitosan/PEO, the increase was almost similar to that on days 3, 7, and 10. A significant increase was noted on day 14; however, the increase was approximately 0.5-fold.

In addition, the cell mineralization pattern on chitosan/PEO and chitosan/PEO/BG nanofibers after 14 days of culturing was qualitatively assessed by FE-SEM/EDX (Figure 10 and 11, respectively). The FE-SEM images revealed the surface

mineralization of cells in the form of distinct nodules for both type of scaffolds. In case of chitosan/PEO/BG nanofibers these nodules were larger in size comparing to the ones in chitosan/PEO nanofibers. Overall, the cell on chitosan/PEO scaffold showed a smoother surface comparing to the cell grown on chitosan/PEO/BG scaffold. Moreover, the EDX results showed the presence of calcium phosphate on surface of merging cell on both scaffolds. Notably, the Ca/P molar ratio on surface of merging cell layer on non-BG-containing scaffold was equal to 1.1 whilst this ratio was measured to be 1.4 (close to 1.5 of HCA) for the cell grown on BG-containing scaffold. These results suggests that cell mineralization occurred in both type of scaffolds, however, the BG-containing scaffold showed a higher level of mineralization due to the presence of BG in the scaffolds [34]. Consistent with the cell mineralization results, the apatite formation and ALP production indicates that BG scaffold had higher potential to induce hMSCs differentiation into osteogenic-like cells; however, further studies on extended time points are needed to clarify its potential.

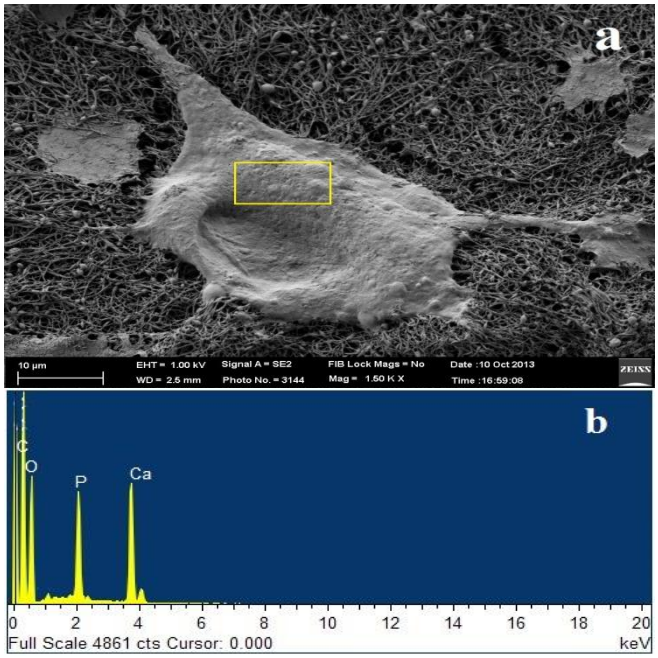

Figure 10. FESEM image of hMSCs grown on the surface of chitosan/PEO scaffold after 14 days (a). EDX spectra of hMSCs in the boxed region which is representing a significant presence of Ca and P on the surface of composite nanofibers after 14 days of seeding (b).

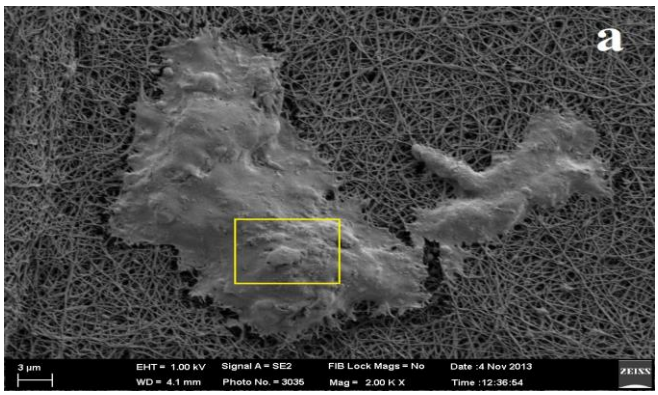

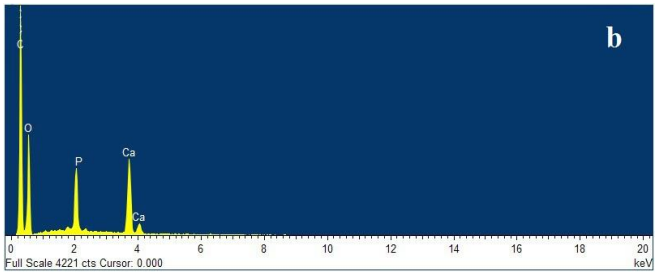

Figure 11. FESEM image of hMSCs grown on the surface of chitosan/PEO/BG scaffold after 14 days (a). EDX spectra of hMSCs in the boxed region which is representing a significant presence of Ca and P on the surface of composite nanofibers after 14 days of seeding (b).

Experimental

Materials

Low-molecular weight chitosan powders (DD ≥75%) were purchased from Sigma-Aldrich; high-molecular weight PEO (PEO-900,000 M_w) was supplied by Acros-Organics; and glacial acetic acid was obtained from R&M Chemicals. Tetraethyl orthosilicate (TEOS, 98%) and triethyl phosphate (TEP, 99%) were purchased from Acros Organics, while sodium nitrate ($NaNO_3$), calcium nitrate tetrahydrate ($CaNO_3.4H_2O$), and nitric acid (HNO_3, 65%) were supplied by R&M Chemicals.

Synthesis of BG particles

BG was fabricated by a sol-gel method proposed by Siqueira [19]; accordingly, fabrication of BG involved hydrolysis and polycondensation of stoichiometric amounts of TEOS, TEP, $NaNO_3$, and $CaNO_3.4H_2O$ to obtain the final composition of SiO_2 as 49.15 mol%, CaO 25.80 mol%, Na_2O 23.33 mol%, and P_2O_5 1.73 mol%. The hydrolysis of TEOS and TEP was performed in 0.1 mol L^{-1} HNO_3 solution using a 8 molar ratio of HNO_3+H_2O/TEOS+TEP. First, TEOS was added to the HNO_3 solution under constant stirring by using an overhead mixer, then other reagents were added to the mixture at 60-min intervals with continuous stirring until the solution reached the gelation point. Next, the gel was kept at room temperature for overnight until it turned translucent. Subsequently, the gel was dried at 130°C for 2 days. Finally, the dried gel was calcinated at 700°C for 3 h with heating at the rate of 1°C min^{-1} , after which the resulting ceramic was ball milled for 12 h until a fine particulate BG ceramic was obtained.

Preparation of electrospun nanofibrous membrane

A suspension of BG particles was prepared by dispersing 0.05 g BG in 4 mL distilled water (1% w/v) and homogenized on an ultrasonic bath for 30 min. Then, PEO was added to 4 mL BG suspension (3 wt%) and agitated by using a magnetic stirrer until the PEO was completely dissolved. Separately, 3 wt% chitosan powder was dissolved in acetic acid/water mixture (80/20 volume ratio). Then, the chitosan solution and PEO/BG solution were mixed together in a 60/40 (chi/PEO) weight ratio and stirred for 1 h until a clear solution was obtained. Finally, electrospinning was performed under the following conditions: 19-gauge needle, 10-cm tip to the collector distance, 0.4 mL/h pump-rate, and 6-kV voltage. The electrospun fibers were then kept in an oven at low

temperature (60°C) for 24 h to allow complete removal of the solvent.

Chemical and physical characterization of nanofibrous membranes

The microstructure of chitosan/PEO/BG nanofibrous composite was studied under a field-emission scanning electron microscope (FE-SEM; High-resolution FEI Quanta 200F; Hitachi; Japan). Furthermore, to study the elemental composition of the scaffolds, energy dispersive X-ray analysis (EDX) was performed by using the EDX-System (S-4800; Hitachi; Japan) attached to the FESEM instrument with accelerating voltage of 5Kv. The functional groups of the composite membranes were identified by fourier transform infrared (FTIR) analysis (Spectrum 400; Perkin Elmer, USA) with a frequency range of 400 to 4000 cm^{-1}. The X-ray diffraction (XRD) patterns of the powder and the composite were obtained by the PAN analytical's Empyrean XRD (USA) with mono-chromated CuKα radiation (λ = 1.54056 A°), operated at 45 kV, 40 mA, a step size of 0.026°, and a scanning rate of 0.1° s^{-1} over a 2θ range from 2° to 90°.

The mechanical properties of the chitosan/PEO/BG and chitosan/PEO nanofibrous membranes were measured at room temperature by using the Instron 3365 machine (USA) at a strain rate of 1 mm/min. All fibrous membranes were processed into rectangular shape by electrospinning of the samples on a cardboard frame with gap dimensions of 35 mm × 19 mm [43]. The ultimate tensile strength was obtained from the stress–strain curve and calculated as the average of 4 samples.

The static water-contact angle of nanofibrous scaffolds was measured by using a video-based optical contact angle measuring instrument (OCA 15EC; DataPhysics Instruments GmbH; Germany). The nanofibers were the carefully coated onto a glass slide. A single droplet of distilled water (2 µL) was applied to the surface of membrane, and the contact angle was measured after 30 s. The measurements were repeated three times at different locations for each sample, and the average value was calculated.

Biomineralization of the electrospun composites was evaluated by examining the ability of the membranes to form a bone-like apatite on their surface on immersion in simulated body fluid (SBF), which was prepared according to the method described earlier [39, 44]. The scaffolds (10 mm × 10 mm) were soaked in 5 mL SBF and incubated at 37°C in a humidified atmosphere of 5% CO_2 for 14 days with daily replacement of the soaking medium. At the end of the soaking period, the samples were removed from the SBF, carefully rinsed with deionized water, and dried at 80°C in vacuum. FE-SEM and EDX were performed to assess the formation of an apatite layer on the surface of nanofibers.

Human mesenchymal stromal cells (hMSCs) culturing

hMSCs were isolated by using a previously described method [45]. Then, the cells were cultured in ABC media (Invitrogen, Carlsbad, CA, USA) supplemented with 15% fetal bovine serum (FBS, Invitrogen), 100 U/mL penicillin (Sigma-Aldrich, USA), and 100 mg/mL streptomycin (Sigma-Aldrich) in tissue-culture flasks at 37°C in a humidified atmosphere of 5% CO_2. When the cells reached near confluence (80–90%), they were detached by trypsin/ethylenediaminetetraacetic acid (EDTA; Cell Applications, San Diego, CA, USA) and then subcultured into the next passage. All cells used in this study were obtained from a control donor and continuously cultured without any re-cryopreservation until a predetermined number of passages were performed. Then, each scaffold was seeded with a cell suspension (2×10^5 cells/ml) and placed in an incubator for 1 h. Finally, 450 µL of medium was added to each well, and the cells were cultured on tissue culture polystyrene as controls.

MTT assay

The cell viability at different time points (3, 7, 10, and 14 days) was performed in a 96-well microplate reader (Becton Dinkinson, Lincoln Park, USA) by the MTT colorimetric assay, and the absorbance was measured at 570 nm on a spectrophotometer (Bio-Tek Instruments, Winooski, USA). The well containing only the MTT solution were considered as the blank reference.

Cell morphology

The scaffolds seeded with hMSCs were stained with Hoechst 33342 blue (Invitrogen, USA) and analyzed by fluorescence microscopy (C-HGFi; Nikon, Japan) after 20 min of incubation at room temperature. For confocal microscopy (TCS-SP5 II; Leica Microsystem, Mannheim, Germany), the post-fixed (2.5% formalin) scaffold samples were dual stained with Hoechst dye and acridine orange. The three-dimensional (3D) image obtained from the incorporation of multiple series of images collected by confocal laser microscopy facilitated investigation of cell infiltration up to 0–80 µm into the scaffolds.

In order to observe the cells adhering to the sample surface after culturing for 1, 3, 5, and 7 days by FE-SEM, the post-fixed scaffolds (2.5% formalin) were dehydrated by using a series of graded ethanol/water solutions (10, 30, 50, 70, 90, and 100%) and kept in a fume hood to dry at room temperature. After the scaffolds were dried, they were sputter coated with platinum and observed.

ALP assay

The differentiation of hMSCs cultured on scaffolds was evaluated by quantifying the ALP activity. After being cultured for 3, 7, 10, and 14 days, on each indicated day, the supernatant was collected and the ALP activity was immediately measured by using a commercial kit (Abcam, USA) according to the manufacturer's protocol. The production of p-nitrophenol and indication of ALP activity was measured using a microplate reader at 405 nm.

Statistical Analysis

The values obtained were averaged and expressed as means ± standard deviation (SD). Statistical differences were determined using SPSS version 10, post-hoc analysis, followed by ANOVA and LSD. The differences were considered statistically significant if the value of p was < 0.05.

Conclusions

Our results suggest that incorporation of BG into chitosan (PEO) nanofibers would lead to the development of a new nanofibrous

composite that may be an appropriate scaffold for tissue engineering due to its improved mechanical and biological properties as compared with that of pure chitosan(PEO) nanofibers.

Acknowledgements

The authors gratefully acknowledge the financial supports from University of Malaya under the HIR-MoE Grant (Reference number - UM.C /625/1/HIR /MOHE /MED/32 account number – H20001-E000071); University of Malaya Research Grant (UMRG), Grant No. RP021/2012B, and Postgraduate research Fund (PPP), Grant No. PG066/2013A .

Notes and references

a Department of Mechanical Engineering, Engineering Faculty, University of Malaya, 50603 Kulala Lumpur, Malaysia.
b Tissue Engineering Group (TEG), Department of Orthopaedic Surgery, NOCERAL, Faculty of Medicine, University of Malaya, Kuala Lumpur-50603, Malaysia.

1. J. M. Holzwarth and P. X. Ma, *Biomaterials*, 2011, **32**, 9622-9629.
2. S. Dong, J. Sun, Y. Li, J. Li, W. Cui and B. Li, *Materials Science and Engineering: C*, 2014, **35**, 426-433.
3. L. Lao, Y. Wang, Y. Zhu, Y. Zhang and C. Gao, *J Mater Sci: Mater Med*, 2011, **22**, 1873-1884.
4. P. Ni, S. Fu, M. Fan, G. Guo, S. Shi, J. Peng, F. Luo and Z. Qian, *International journal of nanomedicine*, 2010, **6**, 3065-3075.
5. M. Kouhi, M. Morshed, J. Varshosaz and M. H. Fathi, *Chemical Engineering Journal*, 2013, **228**, 1057-1065.
6. H. Oudadesse, X.-V. Bui, Y. Le Gal, A. Mostafa and G. Cathelineau, *Int J of biolo and biomed engi*, 2011, **5**, 49-56.
7. Y. Zhang, J. R. Venugopal, A. El-Turki, S. Ramakrishna, B. Su and C. T. Lim, *Biomaterials*, 2008, **29**, 4314-4322.
8. J. Xu, J. Zhang, W. Gao, H. Liang, H. Wang and J. Li, *Materials Letters*, 2009, **63**, 658-660.
9. H.-H. Lee, H.-S. Yu, J.-H. Jang and H.-W. Kim, *Acta biomaterialia*, 2008, **4**, 622-629.
10. S. G. Caridade, E. G. Merino, N. M. Alves, V. d. Z. Bermudez, A. R. Boccaccini and J. F. Mano, *Journal of the Mechanical Behavior of Biomedical Materials*, 2013, **20**, 173-183.
11. M. E. Frohbergh, A. Katsman, G. P. Botta, P. Lazarovici, C. L. Schauer, U. G. Wegst and P. I. Lelkes, *Biomaterials*, 2012, **33**, 9167-9178.
12. S. Srinivasan, R. Jayasree, K. Chennazhi, S. Nair and R. Jayakumar, *Carbohydrate Polymers*, 2012, **87**, 274-283.
13. D. Wang, Y. Zhang and Z. Hong, *Ceramics International*, 2014, **40**, 9799-9808.
14. G. Diogo, V. Gaspar, I. Serra, R. Fradique and I. Correia, *Biofabrication*, 2014, **6**, 025001.
15. W. Pon-On, N. Charoenphandhu, J. Teerapornpuntakit, J. Thongbunchoo, N. Krishnamra and I. Tang, *Materials Science and Engineering: C*, 2014.
16. M. Peter, N. Binulal, S. Nair, N. Selvamurugan, H. Tamura and R. Jayakumar, *Chemical Engineering Journal*, 2010, **158**, 353-361.
17. K.-T. Noh, H.-Y. Lee, U.-S. Shin and H.-W. Kim, *Materials Letters*, 2010, **64**, 802-805.
18. A. R. Boccaccini, M. Erol, W. J. Stark, D. Mohn, Z. Hong and J. F. Mano, *Composites Science and Technology*, 2010, **70**, 1764-1776.
19. R. L. Siqueira, O. Peitl and E. D. Zanotto, *Materials Science and Engineering: C*, 2011, **31**, 983-991.
20. J.-H. Jo, E.-J. Lee, D.-S. Shin, H.-E. Kim, H.-W. Kim, Y.-H. Koh and J.-H. Jang, *Journal of Biomedical Materials Research Part B: Applied Biomaterials*, 2009, **91B**, 213-220.
21. F. S. Shirazi, E. Moghaddam, M. Mehrali, A. A. Oshkour, H. S. C. Metselaar, N. A. Kadri, K. Zandi and N. A. Abu, *Journal of Biomedical Materials Research Part A*, 2014, n/a-n/a.
22. M. L. Gisela and F. M. João, *Biomedical Materials*, 2012, **7**, 054104.
23. W. Pon-On, N. Charoenphandhu, J. Teerapornpuntakit, J. Thongbunchoo, N. Krishnamra and I. M. Tang, *Materials Science and Engineering: C*, 2014, **38**, 63-72.
24. B. S. Purwasasmita and D. Nurdin, *Solids and Structures*, 2013, **2**.
25. M. Ramalingam, P. Vallittu, U. Ripamonti and W.-J. Li, *Tissue Engineering and Regenerative Medicine: A Nano Approach*, CRC Press, 2012.
26. M. Majhi, R. Pyare and S. Singh.
27. O. Peitl Filho and G. P. Latorre, *Journal of biomedical materials research*, 1996, **30**, 509-514.
28. R. Xin, Q. Zhang, J. Chen and Y. Leng, *Biomedical Materials*, 2008, **3**, 041001.
29. J. A. Nychka, S. L. Mazur, S. Kashyap, D. Li and F. Yang, *Jom*, 2009, **61**, 45-51.
30. M. Pakravan, M.-C. Heuzey and A. Ajji, *Biomacromolecules*, 2012, **13**, 412-421.
31. Q.-Z. Chen and G. A. Thouas, *Acta biomaterialia*, 2011, **7**, 3616-3626.
32. H. S. Mansur and H. S. Costa, *Chemical Engineering Journal*, 2008, **137**, 72-83.
33. S. Jebahi, H. Oudadesse, B. Xv, H. Keskes, T. Rebai, A. El Feki and H. El Feki, *African Journal of Pharmacy and Pharmacology*, 2012, **6**, 1276-1287.
34. G. Stanciu, I. Sandulescu, B. Savu, S. Stanciu, K. Paraskevopoulos, X. Chatzistavrou, E. Kontonasaki and P. Koidis, *Journal of Biomedical & Pharmaceutical Engineering*, 2007, **1**, 34-39.
35. G. Toskas, C. Cherif, R.-D. Hund, E. Laourine, B. Mahltig, A. Fahmi, C. Heinemann and T. Hanke, *Carbohydrate Polymers*, 2013, **94**, 713-722.
36. M. Aliabadi, M. Irani, J. Ismaeili, H. Piri and M. J. Parnian, *Chemical Engineering Journal*, 2013, **220**, 237-243.
37. L. Sim, S. Gan, C. Chan and R. Yahya, *Spectrochimica Acta Part A: Molecular and Biomolecular Spectroscopy*, 2010, **76**, 287-292.
38. X. Song, F. Ling, L. Ma, C. Yang and X. Chen, *Composites Science and Technology*, 2013, **79**, 8-14.
39. T. Kokubo and H. Takadama, *Biomaterials*, 2006, **27**, 2907-2915.
40. L. Kong, Y. Gao, G. Lu, Y. Gong, N. Zhao and X. Zhang, *European Polymer Journal*, 2006, **42**, 3171-3179.
41. K. Yamashita, T. Arashi, K. Kitagaki, S. Yamada, T. Umegaki and K. Ogawa, *Journal of the American Ceramic Society*, 1994, **77**, 2401-2407.
42. T. T. Ruckh, K. Kumar, M. J. Kipper and K. C. Popat, *Acta biomaterialia*, 2010, **6**, 2949-2959.
43. E. Tan, S. Ng and C. Lim, *Biomaterials*, 2005, **26**, 1453-1456.
44. M. Mehrali, E. Moghaddam, S. F. S. Shirazi, S. Baradaran, M. Mehrali, S. T. Latibari, H. S. C. Metselaar, N. A. Kadri, K. Zandi and N. A. A. Osman, *ACS Applied Materials & Interfaces*, 2014, **6**, 3947-3962.
45. G. Krishnamurithy, M. R. Murali, M. Hamdi, A. Abbas, H. B. Raghavendran and T. Kamarul, *Ceramics International*, 2014, **40**, 771-777.

